ARTICLES
https://doi.org/10.1038/s41557-018-0107-7
nature chemistry

Formation of the layered conductive magnet $CrCl_2(pyrazine)_2$ through redox-active coordination chemistry

Kasper S. Pedersen[1,2,3*], Panagiota Perlepe[1,2,4,5], Michael L. Aubrey[6], Daniel N. Woodruff[7], Sebastian E. Reyes-Lillo[8,9,10], Anders Reinholdt[11], Laura Voigt[3], Zheshen Li[12], Kasper Borup[13], Mathieu Rouzières[1,2], Dumitru Samohvalov[1,2,18], Fabrice Wilhelm[14], Andrei Rogalev[14], Jeffrey B. Neaton[8,9,15], Jeffrey R. Long[6,16,17] and Rodolphe Clérac[1,2*]

The unique properties of graphene, transition-metal dichalcogenides and other two-dimensional (2D) materials have boosted interest in layered coordination solids. In particular, 2D materials that behave as both conductors and magnets could find applications in quantum magnetoelectronics and spintronics. Here, we report the synthesis of $CrCl_2(pyrazine)_2$, an air-stable layered solid, by reaction of $CrCl_2$ with pyrazine (pyz). This compound displays a ferrimagnetic order below ~55 K, reflecting the presence of strong magnetic interactions. Electrical conductivity measurements demonstrate that $CrCl_2(pyz)_2$ reaches a conductivity of 32 mS cm^{-1} at room temperature, which operates through a 2D hopping-based transport mechanism. These properties are induced by the redox-activity of the pyrazine ligand, which leads to a smearing of the Cr 3*d* and pyrazine π states. We suggest that the combination of redox-active ligands and reducing paramagnetic metal ions represents a general approach towards tuneable 2D materials that consist of charge-neutral layers and exhibit both long-range magnetic order and high electronic conductivity.

Two-dimensional (2D) materials offer a plethora of exciting properties not seen in 3D materials that are central to emergent molecular-scale electronics[1]. However, existing 2D materials such as atom-thick layers or heterostructures of graphene[2] and transition-metal dichalcogenides[3] have limitations, and their simple chemical nature complicates significantly the possibilities to modulate their electronic, magnetic or optical properties for specific applications. Furthermore, almost all these 2D materials are non-magnetic in their pristine forms[4], hampering their use in emerging technologies relying on the quantum spin of transported electrons, such as spintronics[5], magnetoelectrics[6] and multiferroics[7]. In contrast, transition-metal-doped semiconductors are of particular interest for spintronics application due to their near-total spin polarization[8,9]. However, the precise distribution of metal ions is difficult to control, and spatially low-dimensional systems have not been obtained. For molecule-based systems, significant efforts have been devoted to improving and tailoring the characteristics of magnets[10] and conductors[11], and a combination of these properties is typically only found in materials with separate magnetic and conductive sublattices[12,13].

An alternative approach to 2D materials is inspired by reticular molecule-based metal–organic framework (MOF) chemistry[14]. The synthetic engineering of the inorganic and organic modules leads to almost endless possibilities for tuning both the physical properties and anisotropy of the chemical bonding in a 3D crystalline solid. Interestingly, recent reports have shown great promise for the isolation of novel 2D materials as single sheets or van der Waals heterostructures through exfoliation of coordination solids featuring weak dispersion forces between covalently bonded layers[15]. To introduce strong electronic and magnetic communication between spin carriers in such coordination solids, extensive electronic delocalization is essential[16]. Indeed, record high electrical conductivities have been obtained in 2D coordination solids of ditopic or polytopic conjugated organic ligands and transition-metal ions due to strong π–d conjugation between the ligand and metal ion orbitals[17–22]. However, all of these materials are non-magnetic and involve only square-planar coordinated metal ions. To expand the perspective to the ubiquitous octahedrally coordinated metal ions, recent attention has turned towards multidimensional coordination networks involving $Fe^{II/III}$-benzoquinone radical units[23–25]. However, restraining the chemistry to only those, and a few related, redox partners puts significant limitations on the materials that can be exploited. Indeed, many other metal ion–ligand couples are known to exhibit interesting inner-sphere redox reactions. For instance, several

[1]CNRS, CRPP, UMR 5031, Pessac, France. [2]Univ. Bordeaux, CRPP, UMR 5031, Pessac, France. [3]Department of Chemistry, Technical University of Denmark, Lyngby, Denmark. [4]CNRS, ICMCB, UMR 5026, Pessac, France. [5]Univ. Bordeaux, ICMCB, UMR 5026, Pessac, France. [6]Department of Chemistry, University of California Berkeley, Berkeley, CA, USA. [7]Department of Chemistry, University of Oxford, Oxford, UK. [8]Molecular Foundry, Lawrence Berkeley National Laboratory, Berkeley, CA, USA. [9]Department of Physics, University of California Berkeley, Berkeley, CA, USA. [10]Departamento de Ciencias Físicas, Universidad Andres Bello, Santiago, Chile. [11]Department of Chemistry, University of Copenhagen, Copenhagen, Denmark. [12]Department of Physics and Astronomy – Centre for Storage Ring Facilities (ISA), Aarhus University, Aarhus, Denmark. [13]Center for Materials Crystallography, Department of Chemistry and iNano, Aarhus, Denmark. [14]ESRF – The European Synchrotron, Grenoble, France. [15]Kavli Energy Nanosciences Institute at Berkeley, Berkeley, CA, USA. [16]Department of Chemical and Biomolecular Engineering, University of California Berkeley, Berkeley, CA, USA. [17]Materials Sciences Division, Lawrence Berkeley National Laboratory, Berkeley, CA, USA. [18]Present address: Sara Pharm Solutions, Bucharest, Romania.
*e-mail: kastp@kemi.dtu.dk; clerac@crpp-bordeaux.cnrs.fr

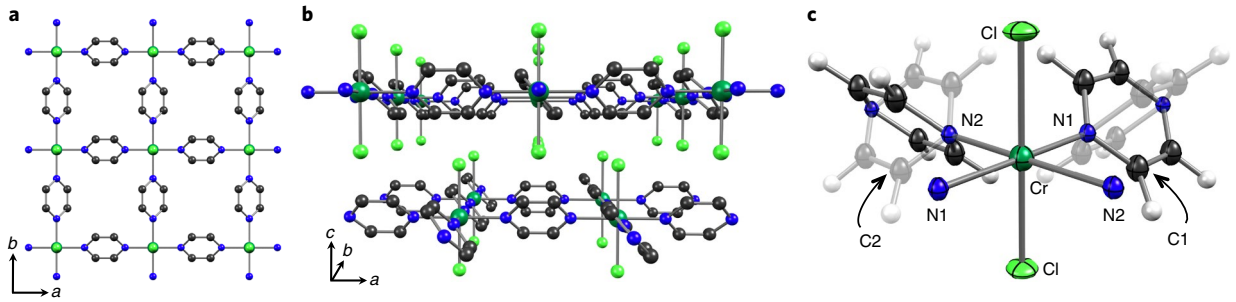

Fig. 1 | Structure of $CrCl_2(pyz)_2$. a, Fragment of the layered structure shown along the Cl–Cr–Cl axis (crystallographic *c* direction), as determined from synchrotron X-ray powder diffraction data at room temperature. **b**, Perspective view of the staggered stacking of the layers perpendicular to the *c* direction. **c**, Thermal ellipsoid plot drawn at 80% probability level showing the positional disorder of the pyrazine rings (dark/light colour). Dark green, Cr; light green, Cl; blue, N; dark grey, C. Hydrogen atoms have been omitted in **a** and **b** for clarity. Selected bond lengths and angles: Cr–N1, 2.003(2) Å; Cr–N2, 2.059(2) Å; Cr–Cl, 2.337(1) Å; N1–C1, 1.349(2) Å; C1–C1, 1.327(3) Å ; N2–C2, 1.333(2) Å ; C2–C2, 1.351(3) Å; $\angle_{dihedral}$C1–N1–Cr–Cl, 42.5°; $\angle_{dihedral}$C2–N2–Cr–Cl, 43.9°.

aromatic amines are known to be redox-active when coordinated to moderately reducing transition-metal ion centres, often resulting in remarkable electronic structures and reactivities for the molecular species[26]. In an attempt to extend this chemistry to coordination networks and to boost both magnetism and electronic conductivity in related 2D materials, we turned our attention to the possible redox-activity of the simple pyrazine (pyz) ligand. This common ditopic ligand is found in thousands of crystallographically characterized coordination networks[27]. Although the pyrazine anion radical can be generated by alkali metal reduction in solution[28] or recently by photon-assisted charge separation in the solid phase[29], the first indication of a transition-metal ion reduction of pyrazine was reported in 1980 by Dunne and Hurst[30]. The purported $[Cr^{III}(Hpyz^{\bullet})]^{3+}$ complex, called 'pyrazine green'[31], formed from the reaction between Cr^{2+} and pyrazine in aqueous solution, was shown to decay quickly to form $[Cr^{III}(pyz)]^{3+}$ and the dihydropyrazinium radical ion $H_2pyz^{\bullet+}$. Inspired by these results, we report the isolation and characterization of a structurally simple layered coordination solid, $\mathbf{CrCl_2(pyz)_2}$, which exhibits both long-range magnetic order and high 2D electronic conductivity.

Results and discussion

The reaction of $CrCl_2$ with a large excess of pyrazine at 200 °C affords a black microcrystalline powder (Supplementary Fig. 1). Elemental analysis of Cr, Cl, N, C and H is consistent with the $CrCl_2(pyz)_2$ formulation (see Methods). The crystal structure (Fig. 1) was solved from synchrotron X-ray powder diffraction data (see Methods and Supplementary Fig. 2). $\mathbf{CrCl_2(pyz)_2}$ crystallizes as a layered structure in the orthorhombic *Immm* space group. The *trans*-$CrCl_2(pyz)_2$ layers are stacked along the crystallographic *c* direction and spaced apart by 5.4 Å. Without indications of a larger supercell from analysis of the powder diffraction pattern, the pyz rings are disordered on two positions imposed by the mirror planes of the *Immm* space group (Fig. 1c). Despite the orthorhombic space group, the 2D network closely approaches the symmetry of a square lattice with Cr···Cr distances of 6.90351(4) and 6.97713(4) Å and Cr–N bond lengths of 2.003(2) and 2.059(2) Å (Fig. 1 caption). On the other hand, the Cr–Cl bond length, 2.337(1) Å, is much shorter than the 2.80 Å found in the related, mononuclear complex *trans*-$[Cr^{II}Cl_2(pyridine)_4]$[32]. Indeed, the metric parameters of the Cr site in $\mathbf{CrCl_2(pyz)_2}$ are in the expected range for Cr^{3+}, as illustrated by *trans*-$[Cr^{III}Cl_2(pyridine)_4](ClO_4)\cdot 1/4H_2O$ (**Cr(III)**), with Cr–N and Cr–Cl bond lengths of 2.1 Å and 2.3 Å, respectively (Supplementary Fig. 3).

Because examples of the apparent absence of a Jahn–Teller axis in Cr^{2+} complexes have been reported[33], further insight into the Cr oxidation state in $\mathbf{CrCl_2(pyz)_2}$ was obtained using X-ray absorption spectroscopy (XAS). XAS spectra were collected at the Cr K-edge of $\mathbf{CrCl_2(pyz)_2}$, and two mononuclear model complexes—**Cr(II)**, (*trans*-$[Cr^{II}Cl_2(NCNH_2)_4]$) and **Cr(III)**, (*trans*-$[Cr^{III}Cl_2(pyridine)_4](ClO_4)\cdot 1/4H_2O$) (Fig. 2)—both featuring a $\{CrN_4Cl_2\}$ chromophore but possessing established +II and +III oxidation respectively. The experimental spectra shown in Fig. 2a and Supplementary Fig. 4 are dominated by the $1s \rightarrow 4p$ transitions, with much weaker pre-edge, dipole-forbidden, $1s \rightarrow 3d$ transitions. The rising edge commences at lower photon energy for **Cr(II)** than for **Cr(III)**, reflecting the stronger binding energy of the 1*s* core electrons in the latter. As has been previously discussed[34], the energetically lowest-lying pre-edge feature, $1s \rightarrow t_{2g}$, is a fingerprint of the Cr oxidation state, which is largely insensitive to the exact ligand field.

The Cr K-edge XAS spectra show that the $\mathbf{CrCl_2(pyz)_2}$ and **Cr(III)** data largely overlap (Supplementary Fig. 4), with an energy of the pre-edge feature for $\mathbf{CrCl_2(pyz)_2}$ that is only 0.2 eV higher than that of **Cr(III)** (Fig. 2a). The X-ray crystallographic and spectroscopic analyses therefore both point towards the presence of Cr^{3+} in $\mathbf{CrCl_2(pyz)_2}$, which necessitates that the pyz scaffold has been reduced by one electron per formula unit during synthesis. Although the crystal structure reveals the presence of two crystallographically different pyrazine ligands, the small differences in the N–C (1%) and C–C (2%) bond lengths do not allow assignment of a localized radical ligand. The Cl K-pre-edge intensity provides direct access to the Cl 3*p* character in the Cr 3*d* orbitals and thus serves as a complementary probe of the Cr electronic structure[35]. The Cl K-edge spectra of $\mathbf{CrCl_2(pyz)_2}$ and **Cr(III)** are strikingly similar (Fig. 2b and Supplementary Fig. 4), whereas the pre-edge intensity for **Cr(II)** is significantly lower. These XAS data thus corroborate unequivocally the similar Cr electronic structure in $\mathbf{CrCl_2(pyz)_2}$ and the archetypal Cr^{3+} complex, **Cr(III)**.

The magnetic susceptibility–temperature product, χT, of $\mathbf{CrCl_2(pyz)_2}$ which amounts to 2.7 $cm^3\,K\,mol^{-1}$ at 400 K (Fig. 3), significantly increases on decreasing the temperature (for example, 3.3 and 4.7 $cm^3\,K\,mol^{-1}$ at 300 K and 200 K, respectively). This thermal behaviour at high temperatures highlights the presence of strong magnetic interactions between spin carriers. A direct comparison of the χT product at 400 K with the Curie constant values (1.9 $cm^3\,K\,mol^{-1}$ for $S=3/2$ Cr^{3+}; 3.0 or 1.0 $cm^3\,K\,mol^{-1}$ for $S=2$ high-spin or $S=1$ low-spin Cr^{2+}, respectively; 2.25 $cm^3\,K\,mol^{-1}$ for uncoupled $S=3/2$ Cr^{3+} and $S=1/2$ pyrazine radical spins; with $g=2$) is thus not straightforward. These magnetic susceptibility data are also poorly described by the Curie–Weiss law, as expected for low-dimensional systems showing strong π–d conjugation and strong magnetic interactions[36]. A sudden increase in the susceptibility is observed at ~55 K, suggesting the existence of a magnetic phase transition (Fig. 3 inset and Supplementary Fig. 5). This result is corroborated by alternating current (a.c.) susceptibility data (Supplementary Fig. 6), which show an abrupt increase

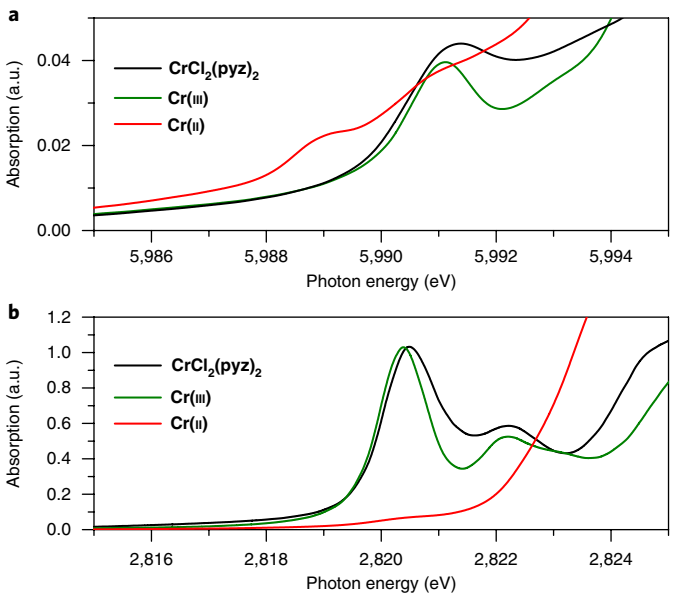

Fig. 2 | XAS at the pre-K-edge region. a, Cr K-edge spectra of **$CrCl_2(pyz)_2$**, **Cr(III)** (*trans*-[$Cr^{III}Cl_2$(pyridine)$_4$](ClO_4)·1/4H_2O) and **Cr(II)** (*trans*-[$Cr^{II}Cl_2(NCNH_2)_4$]) recorded at $T = 3$ K. **b**, Cl K-edge spectra of the same compounds. To facilitate a direct comparison, data were normalized to zero before the edge and to unity far above the edge (Supplementary Fig. 4).

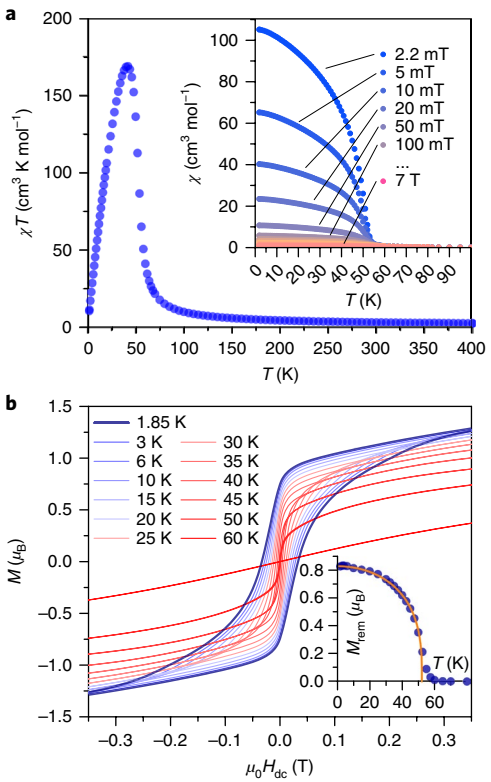

Fig. 3 | Magnetic properties for $CrCl_2(pyz)_2$. a, Temperature dependence of the χT product ($\mu_0 H_{dc} = 0.1$ T). Inset: Temperature dependence of susceptibility at selected d.c. magnetic fields. **b**, Magnetic field dependence of the magnetization obtained with a sweep rate of 30 Oe min^{-1}. Inset: Temperature dependence of the remnant magnetization deduced from the main panel. Solid line: simulation of the temperature dependence of the remnant magnetization, $M_{rem} \propto (1-(T/T_c)^{\alpha})^{\beta}$ with $T_c = 52$ K and $\beta = 0.33$, $\alpha = 2.0$.

in both the in-phase (χ') and out-of-phase (χ'') susceptibilities at ~55 K. The field dependence of the magnetization shows a hysteretic behaviour with a remnant magnetization below ~55 K (Fig. 3 inset and Supplementary Fig. 7), further supporting the assignment of an ordering transition at ~55 K. Notably, this ordering temperature is much higher than that observed for any previously reported pyrazine-based networks. The saturation magnetization at 7 T and 1.85 K amounts to 1.8 μ_B, which is much lower than expected for a ferromagnetically coupled Cr^{3+}-radical pair (~4 μ_B), but is close to the ~2 μ_B expected for antiferromagnetically coupled Cr^{3+} and radical spins. This result supports unambiguously the existence of an ordered ferrimagnetic state below 55 K with strong antiferromagnetic interactions within the 2D coordination network and a parallel alignment of the layer magnetic moments.

Density functional theory (DFT) calculations performed on the simple model fragment, *trans*-[$CrCl_2(pyz)_4$], reveal significant spin density on the dangling pyrazines (Supplementary Fig. 8), and a broken-symmetry calculation provides a rough estimate for the very strong antiferromagnetic Cr^{3+}–pyz radical exchange coupling of around −2,000 cm^{-1} ($J/hc = -2{,}040$ cm^{-1} with the $-2J$ convention). The calculated spin density of the $S = 3/2 - S' = 1/2$ broken-symmetry solution and the corresponding Mulliken population analysis are given in Fig. 4a. The summed spin population on the pyz ligands of −0.68 is close to the ideal value for one electron delocalized on the four pyrazines of the model complex.

To further elucidate the electronic and magnetic ground state of **$CrCl_2(pyz)_2$**, periodic lattice DFT calculations were performed on the experimentally observed ferrimagnetic state and on the likely low-lying antiferromagnetically ordered phase (see Methods). Although both configurations feature antiferromagnetic interactions within the layers, the difference arises from the nature of the interactions between the layers. The DFT-optimized structures with fixed experimental lattice constants are similar for both the ferrimagnetic and antiferromagnetic states, and close to the experimentally determined structure. The optimized C–N–Cr–Cl torsion angles are in the 33–36° range leading to pyrazine rings, which are slightly less tilted than in the experimental structure (43–44°). In both cases, an absolute local magnetic moment of ~2.54 μ_B is found for each Cr^{3+} ion (Cr1 and

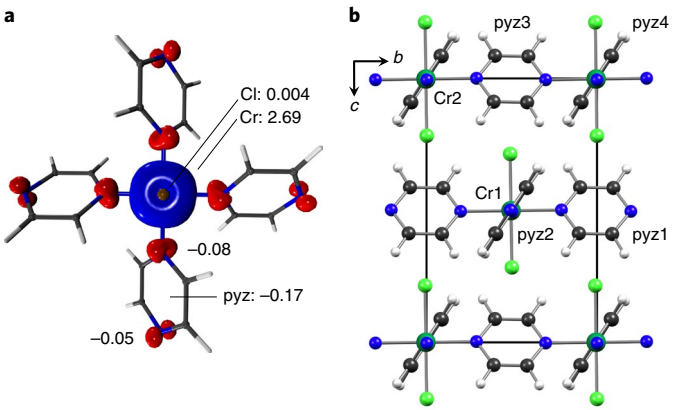

Fig. 4 | DFT calculations. a, DFT-calculated spin density of the broken-symmetry state of the hypothetical [$CrCl_2(pyz)_4$] model complex in the gas phase (isosurface value of ±0.005; blue, positive; red, negative). **b**, DFT-relaxed structure of **$CrCl_2(pyz)_2$** with fixed experimental lattice constants. The labelling highlights structurally distinct units. Calculated spin moments in units of μ_B for the ferrimagnetic (antiferromagnetic) state: Cr1, 2.54 (−2.54); pyz1, −0.32 (0.31); pyz2, −0.28 (0.28); Cr2, 2.54 (2.54); pyz3, −0.26 (−0.26); pyz4, −0.27 (−0.26). The local N and C magnetic moments were −0.12 (0.008) and −0.011 (0.001), respectively, and the Cl moments are negligibly small.

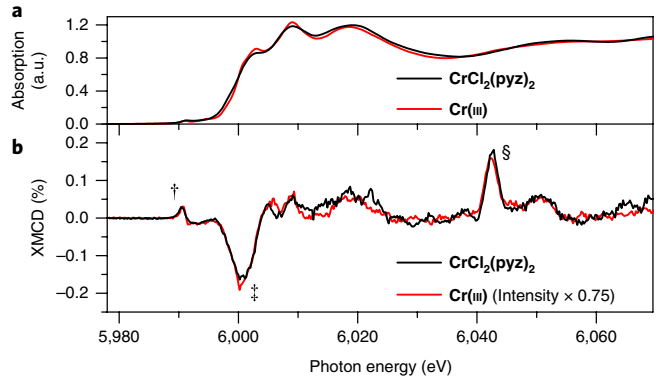

Fig. 5 | XMCD at the Cr K-edge. a, Normalized XAS spectra of **$CrCl_2(pyz)_2$** and **Cr(III)**. **b**, Corresponding XMCD spectra shown as the percentage of the edge jump. These data were obtained at 3 K with a magnetic field of 17 T. The labelled spectral features correspond to pre-edge†, edge‡ and multi-electron excitations§.

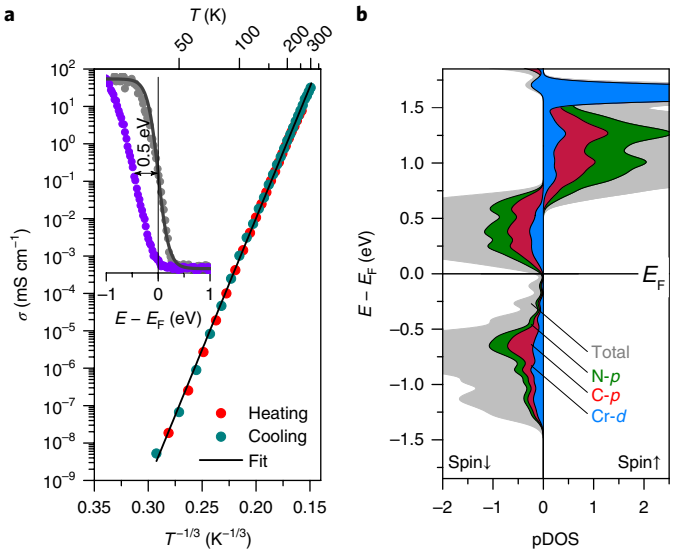

Fig. 6 | Electrical conductivity. a, Temperature dependence of the two-contact conductivity of **$CrCl_2(pyz)_2$**. The solid line is the best fit to the 2D Mott law described in the Methods with $\sigma_0 = 1.2 \times 10^{12}$ mS cm^{-1} and $T_0 = 4.2 \times 10^6$ K. Inset, Fermi edge region of the UV photoelectron spectrum of **$CrCl_2(pyz)_2$** (purple) and the metallic reference (Mo, grey). The solid line is a fit to the Fermi function. **b**, First-principles projected density of states (pDOS) computed using the Heyd–Scuseria–Ernzerhof (HSE) exchange-correlation functional (see Methods) of the ferrimagnetic state of **$CrCl_2(pyz)_2$**, showing the major contributions of the N-*p*, C-*p* and Cr-*d* states to the conduction band.

Cr2 in Fig. 4b), which is significantly reduced from the expected ~3 μ_B for Cr^{3+}. As expected, the local magnetic moments of the pyrazine ligands (pyz*x*, *x* = 1–4, Fig. 4b) are always antiparallel to the nearest Cr moment. The resulting magnetization at saturation for the 2D network is estimated as 1.98 μ_B, in excellent agreement with the experimental data (Supplementary Fig. 7). Thus, the difference between the possible ferrimagnetically and antiferromagnetically ordered states arise only from the respective orientation (parallel and antiparallel, respectively) of the $CrCl_2(pyz)_2$ layer magnetic moments (Fig. 4 caption). We note that these ferrimagnetic and antiferromagnetic states are virtually degenerate at this level of theory (within ~10 cm^{-1} per formula unit), highlighting the very weak interlayer magnetic interactions as compared to the intralayer ones.

In an attempt to determine experimentally the magnitude of the local Cr moment in **$CrCl_2(pyz)_2$**, X-ray magnetic circular dichroism (XMCD) experiments were performed. At the Cr K-edge, the XMCD signal is due to the orbital polarization of the Cr 4*p* and 3*d* states that could be induced either by the intra-atomic spin–orbit interaction of the Cr atoms and (or) by hybridization of the Cr 4*p* states with spin–orbit split states of neighbouring atoms[37]. Given the fact that spin–orbit interactions of the pyz ligand atoms are negligibly small, the second term can be simply neglected. Thus, the observed XMCD signals at the Cr K-edge are due to Cr magnetization only, and their intensity is directly proportional to the magnetic moment of the absorbing atom. The XMCD spectra of **$CrCl_2(pyz)_2$** and **Cr(III)**, shown in Fig. 5, reveal several clear features in the pre-edge († in Fig. 5), at the edge (‡) and also characteristic super-Coster–Kronig multi-electron excitations (§)[38].

The pre-edge signal originates from electric quadrupolar transitions in Cr ions ($1s \rightarrow 3d$) while the negative XMCD peak at the edge involves the 4*p* states, which are polarized by the 3*d* states. The multi-electron excitations also involve transitions from shallow core 3*p* states into 3*d* states and could be also considered as a fingerprint of the 3*d* moment. The XMCD spectra of **Cr(III)** and **$CrCl_2(pyz)_2$** have essentially the same shape, including multielectron excitations, confirming the identical local electronic structure of Cr ions in these systems. Indeed, the intensity of the XMCD spectrum of **Cr(III)** can be scaled by a factor of 0.75 to the **$CrCl_2(pyz)_2$** spectra to yield nearly total overlap. Considering the bulk magnetization of the **Cr(III)** model complex (Supplementary Fig. 9), which saturates at 3.1 μ_B, the local Cr magnetic moment in **$CrCl_2(pyz)_2$** can thus be estimated at 2.3 μ_B. Notably, the Cr moment is strongly reduced from the expected ~3 μ_B, as already concluded from the DFT calculations (2.54 μ_B, vide supra), in excellent agreement with the low experimental value of the **$CrCl_2(pyz)_2$** magnetization at saturation.

Organic mixed-valence systems with strong through-metal coupling were recently reported by some of us as a convenient design principle to yield new conductive MOFs[23]. Similarly, it is straightforward to imagine the highly delocalized open shell frontier states of **$CrCl_2(pyz)_2$** could also allow for bulk electronic conductivity. The black colour of **$CrCl_2(pyz)_2$** was a promising indicator of indispensable low-energy electronic excitations, which are clearly detected by UV–vis–NIR diffuse reflectance spectroscopy (Supplementary Fig. 10), with a strong, very broad absorption band that steadily increases in intensity with decreasing photon energy. These strong absorption features extend into the NIR region, suggesting a quasi-continuous distribution of localized mid-gap states in close energetic proximity[39,40]. Indeed, a broad absorption maximum is observed at 0.5 eV, which could be assigned as an intervalence transfer band (Supplementary Fig. 11)[41]. The temperature dependence of the electrical conductivity, σ, of **$CrCl_2(pyz)_2$** is shown in Fig. 6a. The room-temperature conductivity is $\sigma_{RT} = 32$ mS cm^{-1}, which places **$CrCl_2(pyz)_2$** among the more conducting coordination solids reported so far[16,17]. In contrast to, for example, organic-based charge-transfer salts[11,42], the lack of π–π interactions in **$CrCl_2(pyz)_2$** suggests the presence of a transport mechanism involving both ligand π orbital and metal *d* orbitals. The soft decrease of the conductivity with decreasing temperature suggests an insulating ground state for **$CrCl_2(pyz)_2$** with charge transport dominated by a thermally activated hopping mechanism. Indeed, the temperature dependence of σ could be modelled well by the 2D Mott law invoking a variable-range hopping mechanism (see Methods) commonly used to describe bulk transport of Mott–Hubbard insulators (Fig. 6)[43]. The 2D nature of the transport is further supported by the temperature dependence of the Seebeck coefficient, for which the effect of grain boundaries can be neglected (Supplementary Fig. 12).

The DFT calculations predict a metallic and insulating ground state for the ferrimagnetic and antiferromagnetic phases, respectively, with direct and indirect bandgaps for the antiferromagnetic

phase given by 0.42 and 0.19 eV at Γ and close to Γ (Supplementary Fig. 13). Although UV photoelectron spectroscopy (Fig. 6a inset and Supplementary Fig. 14) agrees with a small optical bandgap (on the order of 0.5 eV), conductivity measurements do not support a metallic ground state (in constrast with the projected density of states (pDOS); Fig. 6b). Most probably, this discrepancy between theory and experiments might have its origin in the structural disorder of the pyrazine ligands, which is not captured in the extended structure DFT calculation[44]. In low-dimensional solids, charge localization is commonly induced by disorder that is difficult to account for in a perfect crystal calculation. The pDOS (Fig. 6b) also supports the potential impact of the pyrazine disorder on the conductivity properties of **$CrCl_2(pyz)_2$** as the frontier orbitals of the valence and conduction bands are dominated by organic C and N 2*p* states. On the other hand, the contributions from the Cr 3*d* states are somewhat smaller and become only dominant from ~1.5 eV above the Fermi level. Notably, the Cr 3*d* states show significant dispersion, which further supports a strong π–*d* hybridization[45].

Conclusions

In this Article we have shown how the redox-activity of a simple ligand, pyrazine, can be used to enhance the electronic and magnetic communication in a layered material, the coordination solid **$CrCl_2(pyz)_2$**. Although structural and X-ray spectroscopic data point toward an oxidation state assignment of +III for the Cr site, its magnetic moment is significantly lower than the expected value for Cr^{3+}. DFT calculations suggest a strong degree of π–*d* conjugation, which, to a certain extent, questions the concept of a metal ion oxidation state, but provides a high magnetic ordering temperature and an unexpectedly high electrical conductivity. In that sense, layers of **$CrCl_2(pyz)_2$** can be considered as a 2D version of the numerous molecular (0D) complexes based on low-valent metal ions, which have shown strong ligand redox-activity and fascinating electronic structures[46]. Similarly, it can be envisioned that 2D coordination solids with improved properties can be designed using strongly reducing transition metal ions in conjunction with organic ligands previously considered to be wholly redox-inactive. The electrically neutral layers of **$CrCl_2(pyz)_2$** also provide the attractive possibility for exfoliation and nanostructuring of this kind of material[47]. Additionally, it should be stressed that **$CrCl_2(pyz)_2$** shows a noticeable resemblance to the cuprates in terms of symmetry, magnetic exchange interactions[48] and π–*d* conjugation[49]. We therefore believe that these results open up exciting new synthetic prospects for novel 2D magnetic conductors derived from metal–organic coordination solids and capable of generating spin-polarized currents in low-dimensional devices.

Methods

Synthesis. All handling of **$CrCl_2(pyz)_2$** was performed under a dry N_2 or Ar atmosphere. A 50 ml Teflon-lined stainless-steel autoclave reactor was charged with $CrCl_2$ (0.20 g, 1.6 mmol; Aldrich, 99.99% trace metal basis) and pyrazine (2.0 g, 25 mmol; Aldrich, ≥99%) and placed in an oven (200 °C) for 24 h. The reactor was cooled to room temperature and the purple-black microcrystalline product of **$CrCl_2(pyz)_2$** was washed with a 20-ml aliquot of *N*,*N*-dimethylformamide and 2 × 20 ml of acetonitrile then dried in vacuo. The yield was 70–75%. Elemental analyses were performed at Mikrolab Kolbe, Mülheim an der Ruhr, Germany. Anal. Calcd. (found) for $C_8H_8Cl_2CrN_4$, Cr: 18.37% (18.12%), Cl: 25.05% (25.33%), C: 33.94% (33.96%), H: 2.85% (2.94%), N: 19.79% (19.57%). Sum: 100% (99.92%). Characteristic Raman (Horiba Scientific XploRA, λ_{inc} = 785 nm) shifts (cm^{-1}): 670; 1,029; 1,221; 1,613.

Spectroscopy. XAS and XMCD spectra were obtained at the ID12 beamline (ESRF, The European Synchrotron). We used the fundamental harmonic of the Apple-II type undulator for experiments at the Cr K-edge, whereas Cl K-edge data were collected using the fundamental harmonic of the Helios-II type undulator. All XAS spectra were recorded using total fluorescence yield detection mode and were subsequently corrected for reabsorption effects. XMCD spectra were obtained as the difference between two consecutive XAS spectra recorded with opposite photon helicities. The XMCD spectra were systematically obtained in both magnetic field directions (at 17 T) to ensure the absence of experimental artefacts. UV–vis–NIR diffuse reflectance spectra were collected using a CARY 5000 spectrophotometer interfaced with Varian Win UV software. The samples were held in a Praying Mantis air-free diffuse reflectance cell. Polyvinylidene fluoride (PVDF) powder was used as a non-adsorbing matrix. FTIR spectra were obtained on a Bruker VERTEX 70v spectrometer. The sample was protected by Ar and opened in the N_2 purged sample compartment and was immediately put on a diamond sample platform from an ATR accessory (MPV-Pro, single reflection; Harrick Scientific Products). UV photoelectron spectra (UPS) were collected at the MATLINE beamline at the ASTRID2 synchrotron located at Aarhus University. Powdered samples were pressed into the pockets on the sample plate (pocket size: 6 mm diameter and 0.5 mm depth; beam spot size at the sample: 0.7 mm × 1 mm). The valence band spectrum was measured by using an incident photon energy of 59.76 eV corresponding to the Fermi edge of the Mo reference.

Magnetic measurements. Magnetic characterization was performed on polycrystalline samples sealed in polypropylene bags (~3 × 0.5 × 0.02 cm; typically 10–20 mg) using an MPMS-XL Quantum Design SQUID magnetometer. All handling of **$CrCl_2(pyz)_2$** was performed under a dry N_2 or Ar atmosphere, but no alterations of its properties were observed after prolonged exposure to atmospheric air. The a.c. susceptibility measurements were performed with an oscillating field of 3 Oe with a frequency from 1 to 1,500 Hz. The field dependence of the magnetization was measured at 100 K to confirm the absence of any bulk ferromagnetic impurities. Magnetic data were corrected for the diamagnetic contributions from the sample and sample holder.

Electrical conductivity. The two-contact variable-temperature conductivity was measured in a home-built two-electrode screw cell with a contact area of 0.04757 cm^2. In an Ar-filled glove box, pellets were pressed between two copper rods with contacts polished to a mirror finish. The screw cell was sealed with Torr Seal low-vapour-pressure epoxy to make an airtight seal. Two-contact conductivity measurements were performed in a Quantum Design MPMS2 SQUID magnetometer with a d.c. transport rod modified to accommodate two 26 AWG silver-coated copper cables sealed at the top of the rod with a gas-tight Swagelok fitting and Torr Seal low-vapour-pressure epoxy. The sample cell was attached to the rod and descended into the cryostat chamber. *I*–*V* profiles were collected with a Bio-Logic SP200 potentiostat with 30 nA current resolution. All data collected were ohmic within a ±1 V window with a very small apparent temperature hysteresis that vanished after thermal cycling and equilibration at 300 K. The resulting *I*–*V* profiles were modelled with Ohm's law, $E \times \sigma = j$, where E is the applied electric field and j is the current density, to determine the sample conductivity σ with units of S cm^{-1}. The temperature dependence of the conductivity was fit to the Mott law relevant for a variable-range hopping mechanism:

$$\sigma(T) = \sigma_0 \exp\left(-\left(\frac{T_0}{T}\right)^{\frac{1}{d+1}}\right)$$

where d is the dimensionality of transport (in the present case of a 2D lattice, $d = 2$), and σ_0 and T_0 (Mott temperature) are empirical constants related to the carrier density and localization length of the hopping electron.

Further synthetic, characterization, magnetic, crystallographic and computational details are provided in the Supplementary Information.

Data availability

All data generated and analysed in this study are included in the Article and its Supplementary Information, and are also available from the authors upon request. Crystallographic information has been deposited in the Cambridge Crystallographic Data Centre under accession codes CCDC 1563526 **($CrCl_2(pyz)_2$)** and CCDC 1563527 **(Cr(iii))**.

Received: 29 September 2017; Accepted: 5 June 2018;
Published online: 10 September 2018

References

1. Novoselov, K. S., Mishchenko, A., Carvalho, A. & Castro Neto, A. H. 2D materials and van der Waals heterostructures. *Science* **353**, aac9439 (2016).
2. Novoselov, K. S. et al. Electric field effect in atomically thin carbon films. *Science* **306**, 666–669 (2004).
3. Chhowalla, M. et al. The chemistry of two-dimensional layered transition metal dichalcogenide nanosheets. *Nat. Chem.* **5**, 263–275 (2013).
4. Huang, B. et al. Layer-dependent ferromagnetism in a van der Waals crystals down to the monolayer limit. *Nature* **546**, 270–273 (2017).
5. Han, W., Kawakami, R. K., Gmitra, M. & Fabian, J. Graphene spintronics. *Nat. Nanotech.* **9**, 794–807 (2014).
6. Tian, Y. et al. Observation of resonant quantum magnetoelectric effect in a multiferroic metal–organic framework. *J. Am. Chem. Soc.* **138**, 782–785 (2016).
7. Gómez-Aguirre, L. C. et al. Magnetic ordering-induced multiferroic behavior in $[CH_3NH_3][Co(HCOO)_3]$ metal–organic framework. *J. Am. Chem. Soc.* **138**, 1122–1125 (2016).

8. Dietl, T., Ohni, H., Matsukura, F., Cibert, J. & Ferrand, D. Zener model description of ferromagnetism in zinc-blende magnetic semiconductors. *Science* **287**, 1019–1022 (2000).
9. Yu, J. H. et al. Giant Zeeman splitting in nucleation-controlled doped CdSe:Mn^{2+} quantum nanoribbons. *Nat. Mater.* **9**, 47–53 (2010).
10. Miller, J. S. Magnetically ordered molecule-based materials. *Chem. Soc. Rev.* **40**, 3266–3296 (2011).
11. Batail, P. Molecular conductors. *Chem. Rev.* **104**, 4887–5782 (2004).
12. Coronado, E., Galán-Mascarós, J. R., Gómez-García, C. J. & Laukhin, V. Coexistence of ferromagnetism and metallic conductivity in a molecule-based layered compound. *Nature* **408**, 447–449 (2000).
13. Coronado, E. & Day, P. Magnetic molecular conductors. *Chem. Rev.* **104**, 5419–5448 (2004).
14. Yaghi, O. M. et al. Reticular synthesis and the design of new materials. *Nature* **423**, 705–714 (2003).
15. Hermosa, C. et al. Mechanical and optical properties of ultralarge flakes of a metal–organic framework with molecular thickness. *Chem. Sci.* **6**, 2553–2558 (2015).
16. Givaja, G., Amo-Ochoa, P., Gómez-García, C. J. & Zamora, F. Electrical conductive coordination polymers. *Chem. Soc. Rev.* **41**, 115–147 (2012).
17. Sun, L., Campbell, M. G. & Dincă, M. Electrically conductive porous metal–organic frameworks. *Angew. Chem. Int. Ed.* **55**, 3566–3579 (2016).
18. Kambe, T. et al. π-Conjugated nickel bis(dithiolene) complex nanosheet. *J. Am. Chem. Soc.* **135**, 2462–2465 (2013).
19. Sheberla, D. et al. High electrical conductivity in Ni_3(2,3,6,7,10,11-hexaiminotriphenylene)$_2$, a semiconducting metal–organic graphene analogue. *J. Am. Chem. Soc.* **136**, 8859–8862 (2014).
20. Huang, X. et al. A two-dimensional π–d conjugated coordination polymer with extremely high electrical conductivity and ambipolar transport behaviour. *Nat. Commun.* **6**, 7408 (2015).
21. Maeda, H., Sakamoto, R. & Nishihara, H. Coordination programming of two-dimensional metal complex frameworks. *Langmuir* **32**, 2527–2538 (2016).
22. Dou, J.-H. et al. Signature of metallic behaviour in the metal–organic frameworks M_3(hexaiminobenzene)$_2$ (M = Ni, Cu). *J. Am. Chem. Soc.* **139**, 13608–13611 (2017).
23. Darago, L. E., Aubrey, M. L., Yu, C. J., Gonzalez, M. I. & Long, J. R. Electronic conductivity, ferrimagnetic ordering, and reductive insertion mediated by organic mixed-valence in a ferric semiquinoid metal–organic framework. *J. Am. Chem. Soc.* **137**, 15703–15711 (2015).
24. DeGayner, J. A., Jeon, I.-R., Sun, L., Dincă, M. & Harris, T. D. 2D conductive iron-quinoid magnets ordering up to T_c = 105 via heterogeneous redox chemistry. *J. Am. Chem. Soc.* **139**, 4175–4184 (2017).
25. Murase, R. et al. Mixed valency in a 3D semiconducting iron-fluoranilate coordination polymer. *Inorg. Chem.* **56**, 9025–9035 (2017).
26. Chirik, P. J. & Wieghardt, K. Radical ligands confer nobility on base-metal catalysts. *Science* **327**, 794–795 (2010).
27. Groom, C. R., Bruno, I. J., Lightfoot, M. P. & Ward, S. C. The Cambridge Structural Database. *Acta Crystallogr. B* **72**, 171–179 (2016).
28. McDowell, C. A., Paulus, K. F. & Rowlands, J. R. Electron-spin resonance spectra of some diazine radical anions. *Proc. Chem. Soc.* **0**, 60–61 (1962).
29. Zhang, X. et al. Stabilizing and color tuning pyrazine radicals by coordination for photochromism. *Chem. Commun.* **52**, 7947–7949 (2016).
30. Dunne, T. G. & Hurst, J. K. Kinetic and thermodynamic properties of chromium(III) complexes containing pyrazine radical ligands. *Inorg. Chem.* **19**, 1152–1157 (1980).
31. Swartz, J. & Anson, F. C. Electrochemistry of the intensely green complexes formed by the reaction of Cr^{2+} with pyrazine ('pyrazine green'), pyrazinecarboxamide, and pyrazinecarboxylic acid. *Inorg. Chem.* **20**, 2250–2257 (1981).
32. Cotton, F. A. et al. Experimental and theoretical study of a paradigm Jahn–Teller molecule, all-*trans*-$CrCl_2(H_2O)_2$(pyridine)$_2$, and the related *trans*-$CrCl_2$(pyridine)$_4$·acetone. *Inorg. Chim. Acta* **235**, 21–28 (1995).
33. Cotton, F. A., Favello, L. R., Murillo, C. & Quesada, J. F. A completely suppressed Jahn–Teller effect in the structure of hexaaquachromium(II) hexafluorosilicate. *J. Solid State Chem.* **96**, 192–198 (1992).
34. Scarborough, C. C. et al. Scrutinizing low-spin Cr(II) complexes. *Inorg. Chem.* **51**, 6969–6982 (2012).
35. Glaser, T., Hedman, B., Hodgson, K. O. & Solomon, E. I. Ligand K-edge X-ray absorption spectroscopy: a direct probe of ligand-metal covalency. *Acc. Chem. Res.* **33**, 859–868 (2000).
36. Miyazaki, A. et al. Crystal structure and physical properties of conducting molecular antiferromagnets with a halogen-substituted donor: (EDO-$TTFBr_2)_2FeX_4$ (X = Cl, Br). *Inorg. Chem.* **46**, 3353–3366 (2007).
37. Solovyev, I. V., Dederichs, P. H. & Mertig, I. Origin of orbital magnetization and magnetocrystalline anisotropy in *TX* ordered alloys (where *T* = Fe, Co and *X* = Pd, Pt). *Phys. Rev. B* **52**, 13419–13428 (1995).
38. Kawamura, N. et al. Multielectron excitations probed by helicity-modulation XMCD a *K*-edge in 3*d* transition metal compounds. *J. Synchrotron Rad.* **8**, 410–412 (2001).
39. Bredas, J. L. & Street, G. B. Polarons, bipolarons, and solitons in conducting polymers. *Acc. Chem. Res.* **18**, 309–315 (1985).
40. Benoit, C., Bernard, O., Palpacuer, M., Rolland, M. & Abadie, M. J. M. Infrared transmission of heavily doped polyacetylene. *J. Phys. Fr.* **44**, 1307–1316 (1983).
41. Dinolfo, P. H., Williams, M. E., Stern, C. L. & Hupp, J. T. Rhenium-based molecular rectangles as frameworks for ligand-centered mixed valency and optical electron transfer. *J. Am. Chem. Soc.* **126**, 12989–13001 (2004).
42. Jérome, D. Organic conductors: from charge density wave TTF-TCNQ to superconducting $(TMTSF)_2PF_6$. *Chem. Rev.* **104**, 5565–5591 (2004).
43. Roth, S. & Carroll, D. *One-dimensional Metals: Conjugated Polymers, Organic Crystals, Carbon Nanotubes and Graphene* (Wiley, New York, 2015).
44. Foster, M. E., Sohlberg, K., Allendorf, M. D. & Talin, A. A. Unraveling the semiconducting/metallic discrepancy in $Ni_3(HITP)_2$. *J. Phys. Chem. Lett.* **9**, 481–486 (2018).
45. Li, W. et al. High temperature ferromagnetism in π-conjugated two-dimensional metal–organic frameworks. *Chem. Sci.* **8**, 2859–2867 (2017).
46. Kaim, W. & Schwederski, B. Non-innocent ligands in bioinorganic chemistry—an overview. *Coord. Chem. Rev.* **254**, 1580–1588 (2010).
47. Rodríguez-San-Miguel, D., Amo-Ochoa, P. & Zamora, F. MasterChem: cooking 2D-polymers. *Chem. Commun.* **52**, 4113–4127 (2016).
48. Bourges, P., Casalta, H., Ivanov, A. S. & Petitgrand, D. Superexchange coupling and spin susceptibility spectral weight in undoped monolayer cuprates. *Phys. Rev. Lett.* **79**, 4906–4909 (1997).
49. Walters, A. C. et al. Effect of covalent bonding on magnetism and the missing neutron intensity in copper oxide compounds. *Nat. Phys.* **5**, 867–872 (2009).

Acknowledgements

K.S.P. thanks the VILLUM Foundation for a VILLUM Young Investigator grant (15374). K.S.P. and R.C. thank the Danish Research Council for Independent Research for a DFF-Sapere Aude Research Talent grant (4090-00201), the University of Bordeaux, the Région Aquitaine, the CNRS, the GdR MCM-2: Magnétisme et Commutation Moléculaires and the MOLSPIN COST action CA15128. M.L.A. and J.R.L. thank the National Science Foundation (grant DMR-1611525) for funding support. K.B. is thankful for funding by the Danish National Research Foundation (Center for Materials Crystallography, DNRF93). D.N.W. thanks the Diamond Light Source Ltd for beam time (I11; EE13284). Theory and computation were supported by the US Department of Energy, Office of Science, Office of Basic Energy Sciences (Theory FWP) Materials Sciences and Engineering Division (DE-AC02-05CH11231). R.C. and J.R.L. are grateful to the France-Berkeley Fund and the CNRS for PICS no. 06485. Work at the Molecular Foundry was supported by the Office of Science, Office of Basic Energy Sciences, of the US Department of Energy under contract no. DE-AC02-05CH11231. J. Bendix, E. Suturina, B. B. Iversen, L. E. Darago, F. Hof, T. Maris and E. Lebraud are thanked for experimental assistance and helpful discussions.

Author contributions

K.S.P. and R.C. conceived, planned and designed the research project. K.S.P., P.P., D.W., A.R. and D.S. executed the syntheses and the chemical and crystallographic analyses. L.V. obtained and analysed the scanning electron microscopy data. M.L.A., M.R., P.P., J.R.L. and R.C. performed and analysed the electrical conductivity experiments. M.R., K.S.P. and R.C. performed and analysed the magnetic susceptibility measurements. Z.L. and K.S.P. obtained and analysed the UPS and NIR–IR data. K.B. and K.S.P. obtained and analysed the Seebeck measurements. S.E.R.-L., J.N. and K.S.P. performed the DFT studies. F.W., A.R., K.S.P., P.P. and R.C. executed the X-ray spectroscopy experiments and analysed the results. All coauthors were involved in the writing of the manuscript and they have all given their consent to its publication.

Competing interests

The authors declare no competing interests.

Additional information

Supplementary information is available for this paper at https://doi.org/10.1038/s41557-018-0107-7.

Reprints and permissions information is available at www.nature.com/reprints.

Correspondence and requests for materials should be addressed to K.S.P. or R.C.

Publisher's note: Springer Nature remains neutral with regard to jurisdictional claims in published maps and institutional affiliations.